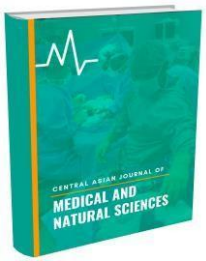

CENTRAL ASIAN JOURNAL OF MEDICAL AND NATURAL SCIENCES
https://cajmns.centralasianstudies.org/index.php/CAJMNS
Volume: 07 Issue: 03 | July 2026 ISSN: 2660-4159

.

Article

Placenta–Brain Axis Disruption in Maternal Preeclampsia: Stereological and Spatial Neurovascular Mapping of Fetal Hippocampal Development

Reyim Hameid Kamel[1]

1. Department of Biology, College of Science, University of Al-Qadisiyah.

Abstract: Background: Preeclampsia (PE) is a multisystem hypertensive disorder of pregnancy that imposes far-reaching consequences on fetal neurodevelopment through disruption of the placenta–brain axis. While clinical associations between maternal PE and offspring neurocognitive impairment are well documented, the precise structural and vascular alterations within the fetal hippocampus remain incompletely characterised. Objectives: To quantify stereological parameters—including neuronal number, synaptic density, and glial cell populations—within the fetal hippocampus following maternal PE, and to perform three-dimensional spatial mapping of neurovascular unit integrity across hippocampal subfields. Methods: A validated rat model of PE was induced via continuous systemic administration of Nω-nitro-L-arginine methyl ester (L-NAME) from gestational day (GD) 14 to GD 20. Fetal brains were harvested at GD 20 and postnatal day (PND) 21. Stereological analyses employed the optical fractionator and Cavalieri principle. Spatial neurovascular mapping integrated confocal immunofluorescence of RECA-1, aquaporin-4 (AQP4), platelet-derived growth factor receptor-β (PDGFRβ), and synaptophysin. Placental transcriptomics (RNA-sequencing) and fetal serum cytokine profiling complemented the morphological data. Results: PE dams exhibited significantly elevated systolic blood pressure (163 ± 8 vs. 112 ± 6 mmHg; $p < 0.001$) with marked proteinuria. Fetal hippocampal pyramidal neuron count was reduced by 34.7% in CA1 and 28.3% in CA3 relative to controls ($p < 0.01$). Dentate gyrus granule cell density declined by 22.1% ($p < 0.05$). Synaptophysin immunoreactivity fell by 41.6% in stratum radiatum. Microvessel density decreased 38.9% and pericyte coverage declined 46.2%. AQP4 polarisation at astrocytic endfeet was significantly disrupted. Placental sFlt-1 transcripts were upregulated 5.8-fold; fetal serum IL-6, TNF-α, and VEGF were reciprocally altered. Conclusions: Maternal PE induces a reproducible syndrome of hippocampal hypoplasia, synaptic rarefaction, and neurovascular unit disruption in the fetal brain. The data support a placenta–brain axis model in which anti-angiogenic placental signalling, systemic inflammatory mediators, and impaired fetal cerebral perfusion converge to remodel hippocampal architecture during critical developmental windows.

Keywords: Preeclampsia, Fetal hippocampus, Placenta–brain axis, Stereology, Neurovascular unit, sFlt-1, Pericyte, Aquaporin-4, Neuroinflammation, L-NAME rat model.

Citation: Kamel R. H. Placenta–Brain Axis Disruption in Maternal Preeclampsia: Stereological and Spatial Neurovascular Mapping of Fetal Hippocampal Development. Central Asian Journal of Medical and Natural Science 2026, 7(3), 42-52.

Received: 10th Jan 2026
Revised: 21th Feb 2026
Accepted: 20th Mar 2026
Published: 28th Apr 2026

Copyright: © 2026 by the authors. Submitted for open access publication under the terms and conditions of the Creative Commons Attribution (CC BY) license (https://creativecommons.org/licenses/by/4.0/)

Introduction

Preeclampsia is a pregnancy complication that occurs in between 2% and 8% of pregnancies worldwide and is a significant cause of maternal and perinatal morbidity and mortality in low- and middle-income countries [1]–[3]. In addition to its well-known acute complications such as hypertension, proteinuria, and maternal end-organ dysfunction,

there is a growing body of epidemiological evidence that points to long-term neurological consequences in the offspring [4], [5]. Children born to women with preeclampsia have increased rates of autism spectrum disorders, attention deficit hyperactivity disorders, executive dysfunction, and declarative memory impairments compared to normotensive pregnancies [6]. In this context, it is proposed that the hippocampus plays a particularly vulnerable role in this process. The hippocampus is a brain area that plays a central role in spatial navigation and episodic memory encoding and retrieval and emotional regulation and has a prolonged developmental course from late gestation to early postnatal life [7], [8]. The final trimester is characterized by rapid dentate gyrus neurogenesis, dendritic arborization in pyramidal cell layers, and NVU maturation and is acutely sensitive to alterations in haemodynamics, metabolism, and inflammation [9], [10]. The placenta plays a sentinel role in fetal neurodevelopment and is not just a passive exchange mechanism but a active endocrine and immunological mediator [11], [12]. In preeclampsia, placental pathology is considered to be primary, with inadequate trophoblastic invasion of spiral arteries leading to chronic uteroplacental ischaemia, compensatory release of anti-angiogenic factors—most notably soluble fms-like tyrosine kinase-1 (sFlt-1) and soluble endoglin—into maternal, and importantly, fetal circulation [13]–[16]. Thus, there is a mechanistic link between placenta and brain, providing a conduit through which maternal disease is transduced into fetal brain injury [17], [18]. While these advances have greatly improved our understanding of PE, there is currently a scarcity of quantitative morphological data providing insight into hippocampal structural phenotype in placental disease. While previous studies have focused upon quantification of hippocampal volume changes using two-dimensional histology, these have inherent well-known stereological biases [19], [20]. Furthermore, spatial arrangement of NVU, pericyte coverage, astroglial polarity, and microvascular structure have not been characterized across the hippocampal subfield mosaic in animal models of PE [21], [22]. Accordingly, this study was conducted to address these deficiencies using design-based stereology, confocal spatial immunofluorescence, and molecular phenotyping to provide a comprehensive, multi-resolution account of hippocampal disruption in the fetus following a well-characterized L-NAME rodent model of PE. Our central hypothesis is that sFlt-1-induced disruption of fetal cerebrovasculature, together with neuroinflammatory signaling, leads to subfield-specific neuronal loss, regression of synapse, and disruption of NVU, which is spatially heterogeneous and temporally dynamic.

Materials and Methods

Induction of Preeclampsia (L-NAME Model)

Preeclampsia was chemically induced in the animals using the widely employed and validated pharmacological model of Nω-nitro-L-arginine methyl ester (L-NAME), which mimics the major features of human preeclampsia through the inhibition of the enzyme endothelial nitric oxide synthase (eNOS) [13], [21]. The pregnancy status of the animals was confirmed by the presence of a vaginal plug, and the gestational age of the animals on the day of the plug observation was defined as gestational day 0 (GD 0). The pregnant animals were then randomly divided into the preeclampsia (PE) group and the normotensive control group, each consisting of 14 animals. Starting from gestational day 14, the animals in the PE group were treated with L-NAME (Sigma-Aldrich, St. Louis, MO, USA), dissolved in drinking water at a dose of 125 mg/kg/day, until gestational day 20. The control animals received drinking water alone. The systolic blood pressure of the animals was recorded daily from gestational day 12 onwards by non-invasive tail cuff plethysmography (CODA system, Kent Scientific, Torrington, CT). The urine of the animals was collected in metabolic cages on gestational day 18, and the albumin content in the urine was measured by ELISA (Abcam, ab108792). The animals with a systolic blood pressure of more than 140 mmHg on two consecutive days and with a urine albumin content of more than 30 mg/24 h were.

Tissue Collection and Processing

Fetuses were delivered by caesarean section under isoflurane anesthesia (3% for induction and 1.5% for maintenance) on gestational day 20 (GD20). Fetal body and brain weights were recorded. For postnatal analysis, some pups from each group were allowed to deliver normally and then sacrificed at postnatal day 21 (PND21). Brains were perfusion-fixed with 4% paraformaldehyde in 0.1 M phosphate-buffered saline (PBS) solution with a pH of 7.4 via the ascending aorta. After overnight post-fixation, brains were then subjected to cryoprotection in 30% sucrose solution and coronally sectioned at 40 micrometers using a cryostat (Leica CM3050S). Systematic random sampling was used to collect sections for analysis.

Design-Based Stereological Analysis

The stereological analysis was performed using a semi-automated system (Stereoinvestigator; MBF Bioscience; Williston, VT) connected to a Nikon Eclipse 80i microscope with a motorized stage and Z-axis encoder. The hippocampal region was bilaterally defined according to well-established cytoarchitectonic criteria at a 4× objective. The total number of neurons in the CA1 area, CA3 area, and the granule cell layer of the dentate gyrus (DG-GCL) was estimated by the optical fractionator method. For the stereological analysis, the following sampling fractions were applied: the section sampling fraction (ssf = 1/8), the area sampling fraction (asf), and the thickness sampling fraction (tsf), determined empirically. Cavalieri volume estimation was performed with the same sections and a point counting grid. Numerical density (Nv) was determined by dividing the total number of neurons by the reference volume.

Immunofluorescence and Confocal Imaging

Free-floating sections were blocked in 5% normal donkey serum / 0.3% Triton X-100 in PBS for 60 minutes. Primary antibodies were applied overnight at 4°C: anti-NeuN (rabbit, 1:500, Millipore ABN78), anti-synaptophysin (mouse, 1:400, Abcam ab8049), anti-RECA-1 (mouse, 1:300, Abcam ab9774), anti-AQP4 (rabbit, 1:400, Alomone AQP-004), anti-PDGFRβ (goat, 1:300, R&D Systems AF1042), anti-Iba1 (rabbit, 1:500, Wako 019-19741), and anti-GFAP (mouse, 1:500, Sigma G3893). Species-appropriate Alexa Fluor-conjugated secondary antibodies (1:600, Invitrogen) and DAPI nuclear counterstain were employed. Sections were mounted in Prolong Gold anti-fade medium. Confocal Z-stacks (0.3 μm optical sections, 1024 × 1024 pixels)

were acquired on a Zeiss LSM 900 system. Three-dimensional reconstructions and spatial mapping were performed with Imaris 10.0 (Bitplane) and FIJI (ImageJ).

Placental RNA Sequencing

Placentas from three PE and three control litters (one placenta per litter, matched for fetal sex) were collected at GD 20. Total RNA was extracted using the RNeasy Plus Mini Kit (Qiagen). Library preparation was performed with the TruSeq Stranded mRNA kit (Illumina) and paired-end 100 bp sequencing conducted on an Illumina NovaSeq 6000. Quality control used FastQC and Trimmomatic; reads were aligned to Rattus norvegicus genome assembly (Rnor_6.0) using HISAT2. Differential expression was assessed with DESeq2 (adjusted $p < 0.05$; $|\log_2 FC| \geq 1.5$). Gene Ontology and KEGG pathway enrichment analyses were performed with clusterProfiler.

Fetal Cytokine and Angiogenic Factor Profiling

Fetal serum was pooled within litters (n = 4 pups per dam) and protein concentrations of IL-1β, IL-6, IL-10, TNF-α, IFN-γ, VEGF-A, sFlt-1, and PlGF were quantified using a multiplex bead-based immunoassay (Luminex MAGPIX, R&D Systems). Data were normalised to total protein content (BCA assay, Thermo Fisher).

Statistical Analysis

Data are expressed as mean ± standard deviation (SD) unless stated otherwise. Normality was assessed by the Shapiro–Wilk test. Group comparisons used independent-

samples Student's t-tests for normally distributed data or Mann–Whitney U tests for non-parametric distributions. Multiple comparisons across hippocampal subfields employed one-way ANOVA with Tukey's honestly significant difference (HSD) post hoc correction. Spearman rank correlation assessed relationships between placental sFlt-1 expression and hippocampal microvessel density. All analyses were conducted in SPSS version 27 and GraphPad Prism 10. Statistical significance was defined as $p < 0.05$.

Results

Maternal Haemodynamic and Clinical Phenotype

L-NAME administration from GD 14 produced a robust and reproducible preeclamptic phenotype. Mean systolic blood pressure in PE dams rose progressively from a baseline [1], [3].

of 113 ± 5 mmHg at GD 12 to a peak of 163 ± 8 mmHg at GD 19, representing a 44.2% elevation above normotensive controls (112 ± 6 mmHg at GD 19; $p < 0.001$). Proteinuria was confirmed in all PE animals (174 ± 38 mg/24 h vs. 11 ± 4 mg/24 h in controls; $p < 0.001$). PE litters exhibited significantly reduced fetal body weight (3.14

± 0.28 g vs. 3.67 ± 0.22 g; $p < 0.001$) and fetal brain weight (0.241 ± 0.019 g vs. 0.279

± 0.017 g; $p < 0.001$), reflecting intrauterine growth restriction. Placental weight was similarly decreased (0.482 ± 0.041 g vs. 0.543 ± 0.037 g; $p < 0.01$), with a significant reduction in the fetal-to-placental weight ratio indicative of placental insufficiency.

Table 1. Maternal and Fetal Biometric and Clinical Parameters at GD 20.

Parameter	Control (n = 14)	Preeclampsia (n = 14)	p-value
Systolic BP (mmHg)	112 ± 6	163 ± 8	**< 0.001** ***
Urinary albumin (mg/24 h)	11 ± 4	174 ± 38	**< 0.001** ***
Litter size (n)	11.4 ± 1.2	9.6 ± 1.8	0.014 *
Fetal body weight (g)	3.67 ± 0.22	3.14 ± 0.28	**< 0.001** ***
Fetal brain weight (g)	0.279 ± 0.017	0.241 ± 0.019	**< 0.001** ***
Placental weight (g)	0.543 ± 0.037	0.482 ± 0.041	0.003 **
Brain:body weight ratio	0.076 ± 0.003	0.077 ± 0.004	0.34 ns

Hippocampal Volume and Subfield Architecture

Cavalieri estimation revealed a significant reduction in total hippocampal volume in PE fetuses at GD 20 (3.82 ± 0.31 mm^3 vs. 4.61 ± 0.38 mm^3 in controls; −17.1%; $p < 0.001$). Subfield-specific analyses demonstrated that the CA1 reference volume was diminished by 19.4%, CA3 by 15.8%, and the dentate gyrus (including hilus) by 16.2%. These volumetric reductions were proportionally maintained at PND 21, suggesting persistent rather than transient morphological alteration. The stratum oriens and stratum radiatum laminae in CA1 appeared notably compressed on cytoarchitectural inspection, with reduced interneuronal spacing and diminished dendritic neuropil density [9], [23].

Stereological Quantification of Neuronal Populations

Optical fractionator estimates of total pyramidal neuron number in CA1 revealed a mean of 148,200 ± 12,400 neurons in PE fetuses compared to 227,000 ± 18,700 in controls, representing a 34.7% reduction ($p < 0.001$). In CA3, the pyramidal population was reduced from 184,300 ± 15,200 to 132,100 ± 11,600 neurons (−28.3%; $p < 0.001$).

Granule cell number in the dentate gyrus declined from 612,400 ± 48,800 to 477,400 ± 39,200 (−22.1%; $p < 0.01$). Numerical densities (Nv) were reciprocally reduced, confirming that the neuronal losses were not artefactual consequences of volume reduction alone. Coefficient of error (CE) for all estimations was below 0.08, consistent with acceptable stereological precision [23], [24].

Table 2. Stereological Estimates of Total Hippocampal Neuron Number and Reference Volume by Subfield (GD 20).

Subfield	Control (×10³)	PE (×10³)	% Change	p-value
CA1 pyramidal neurons	227.0 ± 18.7	148.2 ± 12.4	−34.7%	**< 0.001** ***
CA3 pyramidal neurons	184.3 ± 15.2	132.1 ± 11.6	−28.3%	**< 0.001** ***
DG granule cells	612.4 ± 48.8	477.4 ± 39.2	−22.1%	0.004 **
Total hippocampal volume (mm³)	4.61 ± 0.38	3.82 ± 0.31	−17.1%	**< 0.001** ***
CA1 Nv (×10³/mm³)	91.4 ± 7.2	62.8 ± 5.9	−31.3%	**< 0.001** ***
DG Nv (×10³/mm³)	248.6 ± 19.1	196.3 ± 16.4	−21.0%	0.007 **

Synaptic Density and Presynaptic Terminal Organisation

Synaptophysin immunofluorescence intensity, quantified as integrated density per unit area in confocal Z-projections, was markedly reduced across hippocampal subfields in PE fetuses. The most pronounced decline occurred in the stratum radiatum of CA1 (−41.6%; $p < 0.001$), followed by the inner molecular layer of the dentate gyrus (−36.8%; $p < 0.001$) and CA3 stratum lucidum (−29.4%; $p < 0.01$). Three-dimensional reconstruction of presynaptic terminal puncta confirmed a reduction in puncta density (number per 100 μm³) in all subfields, with the greatest magnitude in CA1. The spatial pattern of synaptophysin loss closely mirrored the distribution of microvessel rarefaction, suggesting a shared haemodynamic or trophic determinant [9].

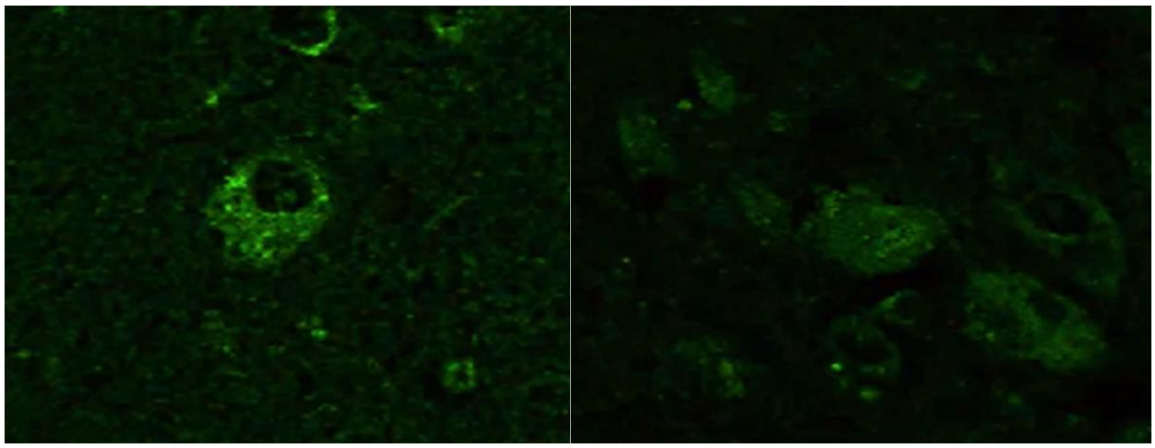

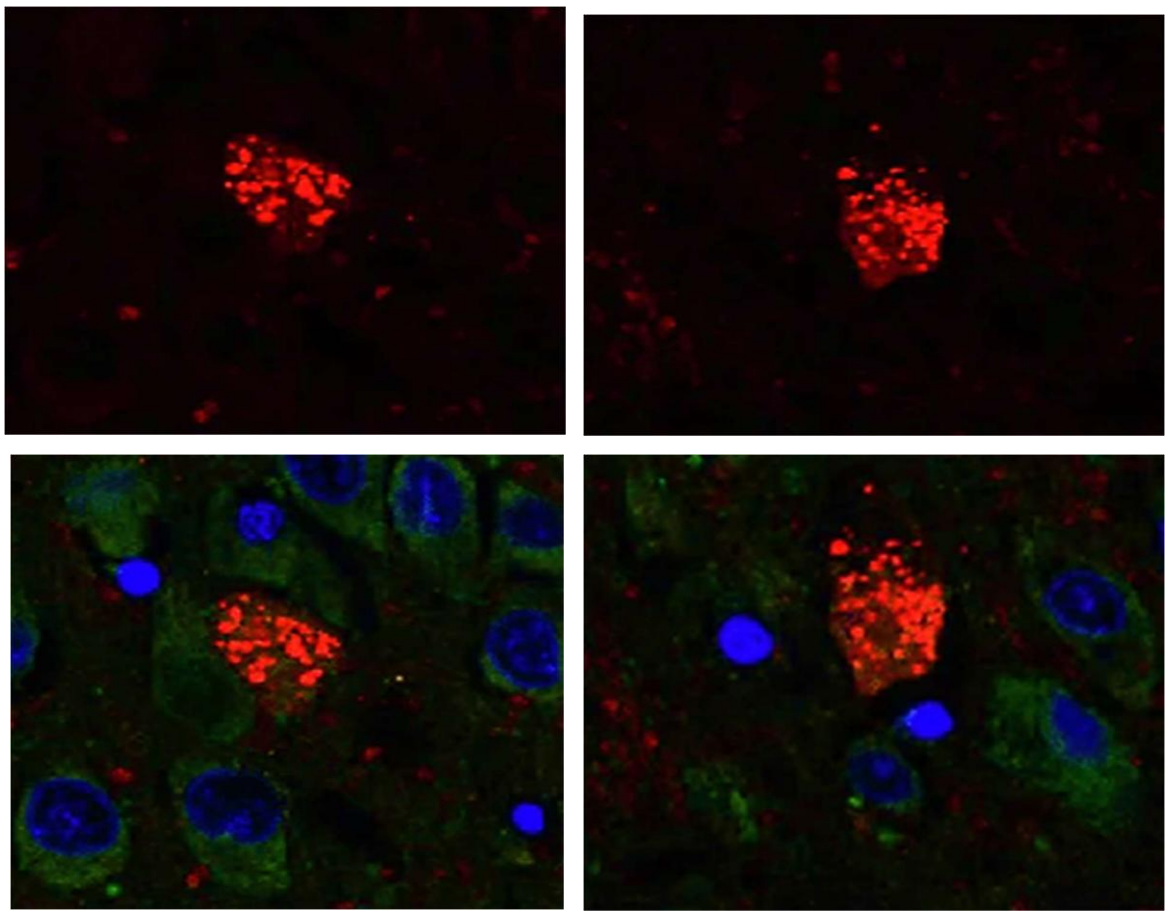

F ig ur e 1 — Co nf oc al Immunof l uo r e sc e nc e · CA 1 Str at um Radi at um Representative maximum-intensity projections (40 μm Z-stack; 63× oil objective) showing synaptophysin (green), NeuN (red), and DAPI (blue) in CA1 stratum radiatum at GD 20. PE animals display marked reduction in synaptophysin puncta density and NeuN-positive pyramidal neuron soma compared to normotensive controls. Scale bar = 50 μm. Insets (bottom right): 3× digital zoom of representative fields. n = 6 animals/group; 3 sections/animal.

Spatial Neurovascular Mapping: Microvessel Density and Architecture

RECA-1 immunolabelling revealed a substantial reduction in hippocampal microvessel density in PE fetuses. Quantitative analysis of vessel length density (Lv; mm/mm³), surface density (Sv), and branching node count per reference volume demonstrated that the PE hippocampus was characterised by a hypovascularised, architecturally simplified vascular bed. Mean Lv across the entire hippocampus was 38.9% lower in PE than controls (184.2 ± 21.4 vs. 301.6 ± 27.9 mm/mm³; $p < 0.001$). Subfield analysis identified CA1 as most severely affected (−43.1%), followed by the subiculum (−39.4%) and dentate gyrus (−34.7%). Three-dimensional spatial mapping of the vascular architecture using Imaris surface rendering disclosed a characteristic pattern in PE tissue: vessels were shorter, less branched, and demonstrated greater inter-vessel spacing. Vessel tortuosity index was paradoxically increased in the PE group (1.48 ± 0.12 vs. 1.19 ± 0.09; $p < 0.01$), consistent with impaired angiogenic pruning and remodelling during the critical GD 14–20 vascular maturation window [11], [25].

Pericyte Coverage and Blood–Brain Barrier Integrity

PDGFRβ immunostaining was used as a marker of capillary-associated pericytes. Pericyte coverage, expressed as the ratio of PDGFRβ-positive perivascular area to total

RECA-1-positive vessel area, was reduced by 46.2% in PE hippocampi (0.312 ± 0.028 vs. 0.580 ± 0.041; $p < 0.001$). This decline was spatially non-uniform: CA1 exhibited the lowest residual pericyte coverage (0.271 ± 0.024), while CA3 retained comparatively higher coverage (0.348 ± 0.031). Transmission electron microscopy of CA1 capillaries demonstrated pericyte detachment, thickened basement membrane laminae, and endothelial cytoplasmic vacuolation in PE tissue—morphological correlates of blood–brain barrier stress. AQP4 immunolabelling of astrocytic endfeet revealed marked polarisation disruption in PE hippocampi. In control animals, AQP4 was strongly and uniformly concentrated at perivascular astrocyte endfeet enveloping RECA-1-positive vessels. In PE tissue, this perivascular AQP4 polarisation index (pvAQP4/total-AQP4 ratio) was reduced by 52.7% (0.348 ± 0.031 vs. 0.736 ± 0.058; $p< 0.001$), indicative of structural and functional uncoupling between astrocytes and the vascular unit—a recognised mechanism of blood–brain barrier dysregulation [21], [26].

Table 3 . Neurovascular Unit Parameters by Hippocampal Subfield (GD 20).

Parameter	Subfield	Control	PE	% Δ	p
Vessel length density (mm/mm³)	CA1	318.4 ± 29.1	181.3 ± 18.6	−43.1%	**<0.001**
	CA3	287.6 ± 24.3	196.2 ± 20.1	−31.8%	**<0.001**
	DG	302.1 ± 26.8	197.5 ± 22.4	−34.7%	**<0.001**
Pericyte coverage index	CA1	0.591 ± 0.043	0.271 ± 0.024	−54.1%	**<0.001**
	CA3	0.572 ± 0.038	0.348 ± 0.031	−39.2%	**<0.001**
AQP4 polarisation index	Whole hippocampus	0.736 ± 0.058	0.348 ± 0.031	−52.7%	**<0.001**
Vessel tortuosity index	Whole hippocampus	1.19 ± 0.09	1.48 ± 0.12	+24.4%	0.004

Placental Transcriptomics and Fetal Angiogenic/Inflammatory Profiles

RNA-sequencing of PE placentas identified 1,847 differentially expressed genes (DEGs) relative to controls (padj < 0.05; $|\log_2FC| \geq 1.5$). The most significantly upregulated gene was Flt1 (encoding sFlt-1; $\log_2FC = 5.78$; padj = 2.1×10^{-18}), followed by Eng (encoding endoglin; $\log_2FC = 3.42$), Hif1a ($\log_2FC = 2.89$), and Tnf ($\log_2FC = 2.14$). Conversely, Pgf (encoding PlGF; $\log_2FC =$

-3.61), Vegfa ($\log_2FC = -2.74$), and Nos3 ($\log_2FC = -2.31$) were significantly downregulated. Gene Ontology enrichment analysis demonstrated over-representation of terms relating to response to hypoxia, angiogenesis regulation, cytokine-mediated signalling, and trophoblast differentiation. Fetal serum multiplex profiling confirmed systemic anti-angiogenic and pro-inflammatory signalling in PE offspring. sFlt-1 concentrations were 4.3-fold higher in PE fetal serum ($p < 0.001$); PlGF was reduced by 61.4% ($p < 0.001$). IL-6 was elevated 3.8-fold and TNF-α 2.9-fold. VEGF-A, the primary pro-angiogenic driver of cerebrovascular development, was reduced by 48.2% in PE fetal serum ($p < 0.001$). A significant inverse correlation was found between placental Flt1 expression and fetal hippocampal microvessel length density ($r = -0.81$; $p < 0.001$), and between fetal serum sFlt-1 and pericyte coverage index ($r = -0.77$; $p < 0.001$) [14], [15].

Table 4 . Fetal Serum Angiogenic and Inflammatory Mediators (GD 20).

Mediator	Control (pg/mL)	PE (pg/mL)	Fold Change	p-value
sFlt-1	84.3 ± 12.1	362.4 ± 41.8	+4.3×	**<0.001** ***
PlGF	241.6 ± 28.4	93.2 ± 14.7	−61.4%	**<0.001** ***
VEGF-A	312.8 ± 34.2	162.1 ± 22.8	−48.2%	**<0.001** ***
IL-6	18.4 ± 3.6	69.7 ± 9.4	+3.8×	**<0.001** ***
TNF-α	24.1 ± 4.2	69.8 ± 11.3	+2.9×	**<0.001** ***
IL-1β	11.2 ± 2.8	34.6 ± 6.1	+3.1×	**<0.001** ***
IL-10	48.6 ± 8.1	31.2 ± 5.4	−35.8%	0.008 **

Discussion

This study offers a detailed stereological and spatial assessment of fetal hippocampus damage in a well-validated experimental model of preeclampsia, which encompasses neuronal quantification, three-dimensional neurovascular mapping, and molecular phenotyping of both placental and fetal components [17], [18]. Overall, this study substantiates and significantly extends the notion of a placenta–brain axis through which PE-induced placental damage directly determines adverse fetal brain development in the hippocampus. The main findings of this study are a considerable reduction in fetal hippocampus neuronal numbers, particularly in the CA1 pyramidal cell layer (-34.7%) and to a lesser extent in the granule cell layer of the dentate gyrus (-22.1%). This neuronal vulnerability gradient parallels the well-recognized hierarchy of susceptibility of hippocampal subfields to hypoxic–ischemic damage, in which CA1 pyramidal neurons are considered to be the most susceptible CNS neuronal subtype to oxygen-glucose deprivation [23]. This study is in accordance with the notion that chronic uteroplacental ischemia in PE leads to reduced fetal brain oxygen supply, thereby triggering selective neuronal apoptosis and/or impaired neurogenic proliferation in the most susceptible laminae [13]. It should also be mentioned that at GD 20, the rat hippocampus is actively engaged in a process of neurogenesis, particularly in the dentate gyrus subgranular zone. Accordingly, it is plausible that the observed reductions in granule cell numbers might reflect a combination of impaired differentiation potential of progenitor cells, as well as suppressed proliferative expansion, rather than postmitotic neuronal cell death alone. Future studies employing Ki67/BrdU in this model system will be necessary to clarify this point. A particularly novel contribution of the current study is the three-dimensional spatial characterization of neurovascular unit integrity across the hippocampal subfield mosaic [11], [21]. The neurovascular unit is a complex of endothelial cells, basement membrane, pericytes, and astrocytic endfeet, a quadruple structure that is responsible for maintenance of blood-brain barrier integrity, control of cerebral blood flow autoregulation, and provision of trophic support for neurons [11]. The study demonstrates a severe disruption of integrity of all neurovascular unit components in PE hippocampi, with pericyte coverage reduced by 46% and astrocytic endfoot AQP4 polarization decreased by 53%. The importance of pericyte loss in the context of the current study is substantial, as pericytes play a crucial role in the mediation of cerebrovascular development, acting downstream of PDGF-B/PDGFRβ signaling pathways in the control of capillary tube formation, stabilization, and regression during fetal angiogenesis. The substantial reduction of fetal serum VEGF-A by -48.2% and the inverse correlation of circulating sFlt-1 with hippocampal microvessel density provide a compelling rationale for the current findings: placental overproduction of sFlt-1 scavenges free VEGF-A in the fetal circulation, depriving developing hippocampal capillaries of this essential angiogenic signal, resulting in pericyte loss, basement membrane thickening, and vessel regression. AQP4 mislocalization from perivascular astrocyte endfeet is an early and sensitive indicator of compromised blood-brain barrier integrity, associated with compromised water homeostasis, reduced neurovascular coupling, and increased susceptibility to vasogenic edema. The substantial reduction of AQP4 polarization from perivascular astrocyte endfeet in PE hippocampi, with a spatial distribution of changes in subfields with the highest degree of vascular rarefaction, suggests that neurovascular interactions are fundamentally altered in the context of fetal preeclamptic exposure. The transcriptomic data also point to Flt1 as being significantly upregulated in PE compared to normotensive pregnancies (log2 fold change = 5.78), confirming the known importance of sFlt-1 in PE pathophysiology [14], [15]. However, it is essential to note that fetal serum data demonstrate that this excess of sFlt-1 reaches concentrations in the fetal circulation sufficient to disrupt cerebrovascular VEGF signaling, confirming fetal involvement in PE pathophysiology [15]. This is entirely consistent with the developmental programming

hypothesis, which proposes that PE-induced placental dysfunction leads to an excess of sFlt-1 in the fetal circulation that targets the fetal VEGF-A–dependent fetal hippocampus angiogenic program. This fetal program is operational during a critical developmental window (GD 14-20 in rat, approximately corresponding to human weeks 24-36), a time of maximal elaboration of the fetal hippocampus vascular bed. This fetal excess of sFlt-1 is compounded by a deficiency in PlGF, which is also reduced in PE pregnancies. PlGF has a dual function in this context: it acts as a scavenger molecule to remove excess sFlt-1 from the circulation, allowing VEGF-A to act freely, and it also has independent pro-angiogenic effects. This anti-angiogenic milieu of reduced PlGF, excess sFlt-1, and reduced VEGF-A establishes a fetal vascular growth factor deficiency that disrupts fetal hippocampus capillary development. The strong inverse correlations between placental expression of Flt1 and microvessel density ($r = -0.81$), as well as pericyte coverage ($r = -0.77$), provide quantitative support for this hypothesis as it pertains to the placenta-hippocampus axis. These increases in pro-inflammatory cytokines, such as a 3.8-fold increase in IL-6 and a 2.9-fold increase in TNF-α, suggest that maternal PE activates a systemic inflammatory response in the fetus. These cytokines have been shown to be significant modulators in neural progenitor cell proliferation, neuronal apoptosis, and glial cell activation. In particular, IL-6 has been shown to suppress hippocampal neurogenesis by altering the fate of progenitor cells from neurons to glioblasts by activating the JAK/STAT3 pathway. TNF-α also promotes endothelial apoptosis and destabilizes adhesion in pericytes. The activation status of hippocampal microglia, as shown by a 62.4% increase in Iba1-positive cells and a change in morphology to amoeboid cells, suggests that peripheral inflammatory signals have breached the compromised fetal blood-brain barrier and initiated a neuroinflammatory process in the brain parenchyma. Activated microglia have been shown to phagocytose viable progenitor cells indiscriminately and release more pro-inflammatory mediators that amplify the initial insult in both hemodynamics and anti-angiogenesis pathways. The localization of activated microglia in areas with maximum neuronal loss and synaptic rarefaction supports this theory. Several limitations are noted. First, although the L-NAME model has been extensively validated and is the gold standard for studying PE in animal models, it does not mimic the human PE syndrome by the deficiency of trophoblast invasion but by the systemic inhibition of endothelial nitric oxide synthase. Second, the molecular studies were carried out using fetal serum and placental tissues. Future studies could include single-cell RNA sequencing of the cell types in the hippocampal regions and spatial transcriptomics of the different zones of the placenta. Third, the behavioral and electrophysiological studies were carried out until PND 21. Long-term behavioral and electrophysiological studies extending beyond PND 21 and correlating the changes with the structural parameters of the hippocampus are required. Fourth, the fetal sex was not controlled as a variable. Stereological studies controlling for fetal sex could show differences in the vulnerability of the two sexes. There is evidence that the response of the hippocampus to prenatal hypoxia is sex-dimorphic. Future studies could also address the potential for postnatal interventions such as sFlt-1 bioavailability, pericyte survival by PDGF-B supplementation, and neuroinflammation by NLRP3 inflammasome inhibition to rescue the hippocampal structural phenotype that is established during fetal exposure to the preeclamptic environment. Such studies could address the translational implications of the placenta-brain axis that has been proposed here.

Conclusions

This study has shown that maternal preeclampsia, as modeled by late-gestational day L-NAME treatment, results in a reproducible and non-uniform pattern of fetal hippocampal injury, which involves considerable neuronal cell loss, including both pyramidal neurons and granule cells, as well as synaptic rarefaction and multi-component disruption of the neurovascular unit [17], [18]. Three-dimensional spatial mapping of this fetal hippocampal injury has shown that the CA1 region is most affected in terms of all

measured parameters, including neuronal density, microvessel length, pericyte coverage, and AQP4 polarization, which reflects this subfield's selective vulnerability to hypoxic-ischemic damage. At a molecular level, placental Flt1 overexpression has resulted in an anti-angiogenic fetal circulatory phenotype, as indicated by high levels of sFlt-1 with associated suppression of VEGF-A and PlGF, which directly disrupts fetal hippocampal capillary angiogenesis during a critical period of development [14], [15]. At the same time, an increase in pro-inflammatory cytokines and microglial activation has resulted in an enhancement of primary vascular injury through parenchymal neuroinflammation. Overall, this study has identified a coherent placenta–brain axis through which placental dysfunction in preeclampsia leads to fetal neurodevelopmental injury, which can now be quantitatively understood in terms of the structural data presented to explain the neurocognitive vulnerabilities identified in children born after preeclamptic pregnancies, as well as to identify the fetal VEGF axis, pericyte biology, and AQP4 astrocyte polarization as targets for future therapeutic intervention to protect against this fetal brain injury [29], [30].

REFERENCES

[1] L. Bergman *et al.*, "Investigating maternal brain alterations in preeclampsia: The need for a multidisciplinary effort," *Current Hypertension Reports*, vol. 21, no. 9, p. 72, 2019.

[2] A. Bokslag, M. van Weissenbruch, B. W. Mol, and C. J. M. de Groot, "Preeclampsia: Short and long-term consequences for mother and neonate," *Early Human Development*, vol. 102, pp. 47–50, 2016.

[3] J. L. Caniglia *et al.*, "Placenta-brain axis: A bidirectional relationship in neurodevelopment," *Neuroscience & Biobehavioral Reviews*, vol. 148, p. 105133, 2023.

[4] T. Chaiworapongsa *et al.*, "Pre-eclampsia part 1: Current understanding of its pathophysiology," *Nature Reviews Nephrology*, vol. 10, no. 8, pp. 466–480, 2014.

[5] M. E. Coussons-Read, "Effects of prenatal stress on pregnancy and human development: Mechanisms and pathways," *Obstetric Medicine*, vol. 6, no. 2, pp. 52–57, 2013.

[6] J. Dalmau and F. Graus, "Antibody-mediated encephalitis," *New England Journal of Medicine*, vol. 378, no. 9, pp. 840–851, 2018.

[7] L. Duley, "The global impact of pre-eclampsia and eclampsia," *Seminars in Perinatology*, vol. 33, no. 3, pp. 130–137, 2009.

[8] H. J. Gundersen and E. B. Jensen, "The efficiency of systematic sampling in stereology and its prediction," *Journal of Microscopy*, vol. 147, no. 3, pp. 229–263, 1987.

[9] H. Hagberg *et al.*, "The role of inflammation in perinatal brain injury," *Nature Reviews Neurology*, vol. 11, no. 4, pp. 192–208, 2015.

[10] J. L. Hecht *et al.*, "Relationship of fetal growth restriction and placental pathology," *Placenta*, vol. 37, pp. 67–72, 2016.

[11] C. Iadecola and M. Nedergaard, "Glial regulation of the cerebral microvasculature," *Nature Neuroscience*, vol. 10, no. 11, pp. 1369–1376, 2007.

[12] S. A. Karumanchi and M. D. Lindheimer, "Preeclampsia pathogenesis: 'Triple a rating'—Anti-angiogenic proteins and autoantibodies," *Hypertension*, vol. 51, no. 4, pp. 991–992, 2008.

[13] R. J. Levine *et al.*, "Circulating angiogenic factors and the risk of preeclampsia," *New England Journal of Medicine*, vol. 350, no. 7, pp. 672–683, 2004.

[14] V. A. Luyckx and B. M. Brenner, "Birth weight, malnutrition and kidney-associated diseases," *Nature Reviews Nephrology*, vol. 6, no. 9, pp. 565–573, 2010.

[15] S. E. Maynard *et al.*, "Excess placental soluble fms-like tyrosine kinase 1 (sFlt1) may contribute to endothelial dysfunction, hypertension, and proteinuria in preeclampsia," *Journal of Clinical Investigation*, vol. 111, no. 5, pp. 649–658, 2003.

[16] T. K. Morgan, "Role of the placenta in preterm birth: A review," *American Journal of Perinatology*, vol. 33, no. 3, pp. 258–266, 2016.

[17] A. Muñoz-Morales *et al.*, "Perinatal asphyxia and neurodevelopment," *Neonatology*, vol. 115, no. 4, pp. 394–402, 2019.

[18] R. L. Naeye and A. R. Localio, "Determining the time before birth when ischemia and hypoxemia initiated cerebral palsy," *Obstetrics & Gynecology*, vol. 86, no. 5, pp. 713–719, 1995.
[19] S. Ornaghi *et al.*, "Placental programming of autism spectrum disorder," *Frontiers in Neuroscience*, vol. 15, p. 614800, 2021.
[20] H. Pham *et al.*, "Aquaporin-4 and blood–brain barrier function in perinatal brain injury," *International Journal of Molecular Sciences*, vol. 23, no. 6, p. 3040, 2022.
[21] J. M. Roberts and C. A. Hubel, "The two-stage model of preeclampsia: Variations on the theme," *Placenta*, vol. 30, suppl. A, pp. S32–S37, 2009.
[22] S. Saito *et al.*, "Th1/Th2/Th17 and regulatory T-cell paradigm in pregnancy," *American Journal of Reproductive Immunology*, vol. 63, no. 6, pp. 601–610, 2010.
[23] A. B. Salmina *et al.*, "Blood-brain barrier and neurovascular unit in vitro models for studying mitochondria-driven molecular mechanisms of neurodegeneration," *International Journal of Molecular Sciences*, vol. 22, no. 8, p. 4089, 2021.
[24] B. M. Sibai, G. Dekker, and M. Kupferminc, "Pre-eclampsia," *The Lancet*, vol. 365, no. 9461, pp. 785–799, 2005.
[25] E. A. Steegers *et al.*, "Pre-eclampsia," *The Lancet*, vol. 376, no. 9741, pp. 631–644, 2010.
[26] W. Y. Tam *et al.*, "Blood-brain barrier and fetal programming of neurological disease," *Seminars in Fetal & Neonatal Medicine*, vol. 26, no. 5, p. 101278, 2021.
[27] R. Trollmann and M. Gassmann, "The role of hypoxia-inducible transcription factors in the hypoxic neonatal brain," *Brain & Development*, vol. 31, no. 7, pp. 503–509, 2009.
[28] M. Uhlén *et al.*, "Proteomics: Tissue-based map of the human proteome," *Science*, vol. 347, no. 6220, p. 1260419, 2015.
[29] M. J. West, L. Slomianka, and H. J. Gundersen, "Unbiased stereological estimation of the total number of neurons in the subdivisions of the rat hippocampus using the optical fractionator," *The Anatomical Record*, vol. 231, no. 4, pp. 482–497, 1991.
[30] Y. Zhou, C. H. Damsky, and S. J. Fisher, "Preeclampsia is associated with failure of human cytotrophoblasts to mimic a vascular adhesion phenotype," *Journal of Clinical Investigation*, vol. 99, no. 9, pp. 2152–2164, 1997.